CHEMISTRY

π-π stacking interactions: Non-negligible forces for stabilizing porous supramolecular frameworks

Ji-Hua Deng[1,2]*, Jie Luo[2]*, Yue-Lei Mao[2]*, Shan Lai[2], Yun-Nan Gong[2], Di-Chang Zhong[1,2†], Tong-Bu Lu[1]

Revealing the contribution of π-π stacking interactions in supramolecular assembly is important for understanding the intrinsic nature of molecular assembly fundamentally. However, because they are much weaker than covalent bonds, π-π stacking interactions are usually ignored in the construction of porous materials. Obtaining stable porous materials that are only dependent on π-π stacking interactions, despite being very challenging, could address this concern. Here, we present a porous supramolecular framework (π-1) stabilized only by intermolecular π-π stacking interactions. π-1 shows good thermal and chemical stability not only in various organic solvents but also in aqueous solution in a broad pH range. Furthermore, featuring one-dimensional channels with dangling thiolate groups, π-1 exhibits excellent Hg^{2+} removal performance, with adsorption capacity as high as 786.67 mg g^{-1} and an adsorption ratio as high as 99.998%. In addition, π-1 also shows high adsorption selectivity to Hg^{2+} in the presence of a series of interfering ions.

INTRODUCTION

Pioneered by Pedersen, Lehn, and Cram who were awarded the 1987 Nobel Prize in chemistry (*1*–*3*), supramolecular chemistry has been greatly developed in the past several decades. By Lehn's definition, supramolecular chemistry refers to the domain of chemistry beyond that of molecules (*4*). It focuses on molecular assemblies assembled with a number of discrete molecular components through intermolecular weak and reversible noncovalent interactions. These interactions involve hydrogen bond, π-π stacking, hydrophobic association, electrostatic interactions, van der Waals forces, and so on. In contrast to a single covalent bond with an energy of more than 200 kJ/mol, noncovalent interactions were assumed to be much weaker (*5*). A hydrogen bond usually has an energy of 25 to 40 kJ/mol (*6*), and other noncovalent interactions have energies lower than 10 kJ/mol (*7*). In supramolecular compounds, the hydrogen bond is the main and most common intermolecular noncovalent interaction. It usually cooperates with other noncovalent interactions to stabilize the supramolecular networks. Because of the coexistence of these noncovalent interactions, it is difficult to differentiate their contributions to the stability of supramolecular assembly. The clear differentiation helps in understanding the intrinsic nature of molecular assembly fundamentally, particularly for macromolecules in biological systems (*8*). Therefore, despite the great challenge of not having a related example reported to the best of our knowledge, the assembly of supramolecular networks being merely dependent on one type of noncovalent interactions is very meaningful.

Hydrogen-bonded organic frameworks (HOFs) are a class of newly emerged crystalline porous materials (CPMs) (*9*–*20*). In contrast to classic CPMs such as inorganic zeolites (*21*), metal-organic frameworks (MOFs) (*22*), and covalent organic frameworks (COFs) (*23*), HOFs are obviously out of the ordinary, as they are classic supramolecular compounds, where hydrogen bonds contribute to their framework stability, as can be derived from the term itself. Although called HOFs, all reported HOFs are stabilized not merely by hydrogen bonds. Other noncovalent interactions, especially π-π stacking interactions, also give assistance to support porous structures. In some HOFs, π-π stacking even serves as the main intermolecular interactions instead of hydrogen bonds to stabilize the frameworks (*24*–*28*). Therefore, besides hydrogen bonds, π-π stacks are also important intermolecular interactions in supramolecular assembly despite the fact that they are often ignored, as they are relatively weaker.

To demonstrate the contribution of π-π stacks in supramolecular networks well, the emergence of stable CPMs that are only dependent on π-π stacking interactions, namely, π frameworks, is convincing. Undoubtedly, the assembly of a π framework is much more challenging than those of MOFs, COFs, and even HOFs in which diverse noncovalent interactions cooperatively contribute to their stability. Therefore, it is expected that no π framework with permanent porosity has been reported to date. Here, we present a π framework that may identify the contribution of π-π stacking interactions in supramolecular assembly. This π framework is based on a Zn(II) mononuclear complex, $[Zn(phen)_2L]\cdot(3CH_3OH\cdot 6H_2O)$ [**π-1**, H_2L = 1-(4-carboxyphenyl)-5-mercapto-1*H*-tetrazole]. Thorough structural analyses revealed that the framework of **π-1** is only stabilized by intermolecular π-π stacking interactions. More impressively, **π-1** shows good thermal and chemical stability, as well as excellent Hg^{2+} removal performance in aqueous solution due to its thiolate group–modified pore surface.

RESULTS

Synthesis and structure determination

Self-assembly of $Zn(Ac)_2\cdot 2H_2O$, phen, and H_2L in a molar ratio of 2:1:1 at 105°C for 72 hours under solvothermal conditions resulted in a clear solution. This solution was allowed to stand at room temperature for 2 to 3 days, leading to the formation of rod-like crystals of **π-1** in 73% yield (fig. S1, A to C). The infrared (IR) spectra of H_2L **π-1** and activated **π-1** were measured in attenuated total refraction (ATR) mode and transmittance mode, respectively. As shown in fig. S1 (D to G), a peak at 2542 cm^{-1} assigned to the stretching vibration of the —SH group is obviously observed in the IR spectra of H_2L. After combining with Zn(II) to form **π-1**, this peak disappears, indicating

[1]Institute for New Energy Materials and Low Carbon Technologies, School of Materials Science and Engineering, and School of Chemistry and Chemical Engineering, Tianjin University of Technology, Tianjin 300384, China. [2]School of Chemistry and Chemical Engineering, Gannan Normal University, Ganzhou 341000, China.
*These authors contributed equally to this work.
†Corresponding author. Email: zhong_dichang@hotmail.com

the deprotonation of —SH (*29*). In addition, the —COOH characteristic absorption at 1693 cm^{-1} red shifts to 1628 cm^{-1}, demonstrating that the —COOH of H_2L deprotonates and participates in the coordination to Zn(II). These observations indicate that in **π-1**, both carboxylic and thiol groups of H_2L are deprotonated. The generated L^{2-} binds with Zn(II) to form a neutral coordination unit. This result was further confirmed by ion chromatography analysis, as no acetate (Ac^-) was detected in the water solution where **π-1** was immersed for 24 hours (fig. S1H).

Single-crystal x-ray diffraction (XRD) analysis showed that **π-1** crystallizes in the trigonal *R*-3 space group (table S1; see the Supplementary Materials). The central metal Zn(II) ion coordinates with two carboxylic O atoms from one L^{2-} ligand and four N atoms from two phen, generating a six-coordinated mononuclear Zn(II) structural unit (Fig. 1A). Two phen rings of the structural unit respectively stack with two phen rings of two adjacent structural units by strong π-π interactions to form a one-dimensional (1D) supramolecular chain building block along the *c* axis (Fig. 1B). Each supramolecular chain building block further connects with four other equivalent chain building blocks through strong π-π interactions between a tetrazolyl ring and a phen ring, as well as between an aromatic ring and a phen ring (Fig. 1C), resulting in a 3D porous supramolecular framework with 1D thiolate group–modified hexagonal channels (Fig. 1D and fig. S2A). The window size of the channel is about 7.5 Å by 7.5 Å, which is filled with lattice CH_3OH and H_2O molecules, as inferred by elemental analysis and thermogravimetric (TG) analysis (presented below).

On the basis of the above structural analyses, it is clearly seen that the stability of **π-1** is dependent on a number of π-π stacking interactions between conjugated organic groups of the mononuclear

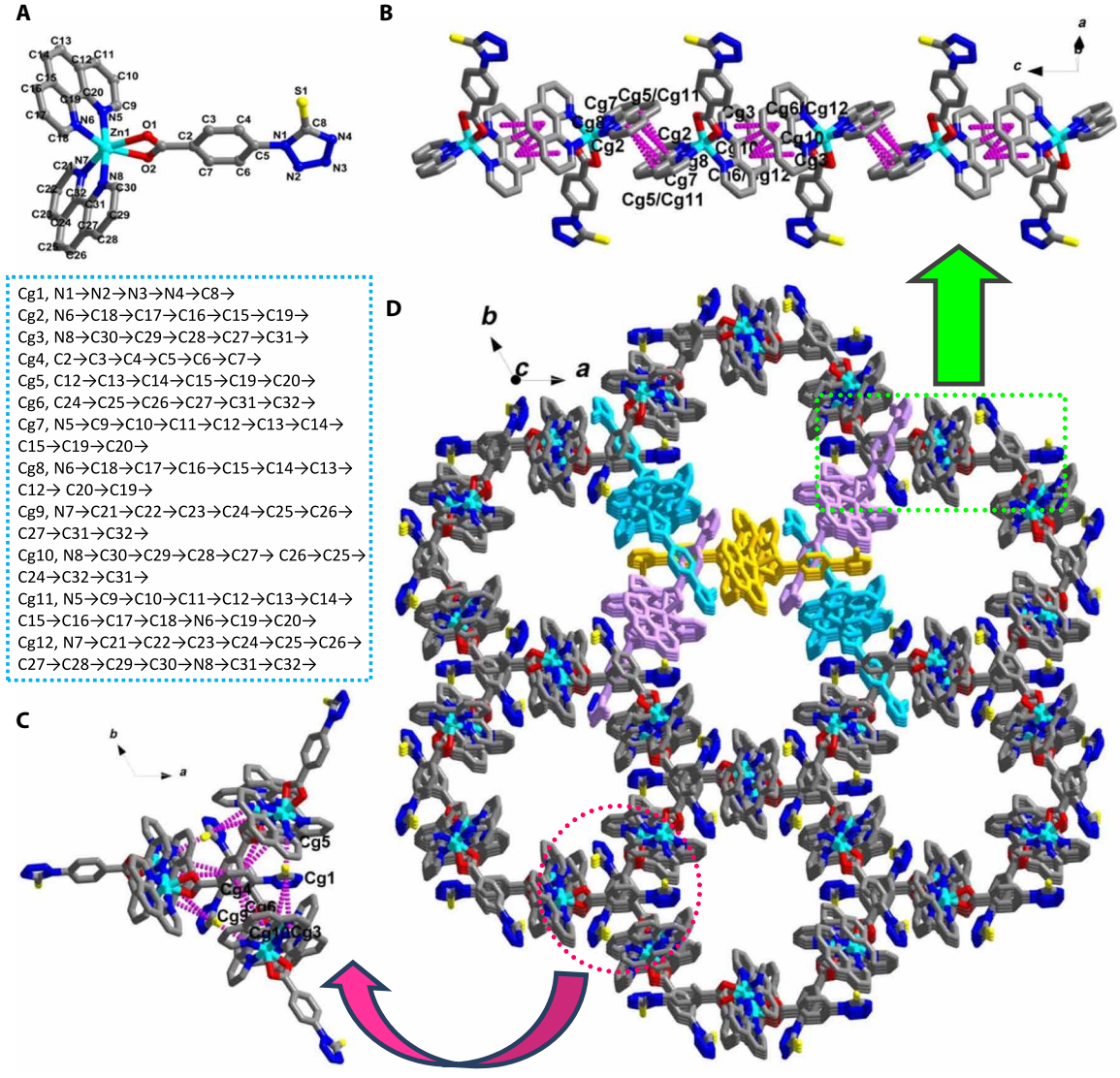

Fig. 1. Crystal structures of π-1. (**A**) Mononuclear Zn(II) structural unit in **π-1**. (**B**) The building block of **π-1** viewed along the *b* axis, showing the strong π-π stacking interactions between phen rings. The selected distances (*D*) between ring centroids are as follows: $D_{Cg2\text{-}Cg5}$ = 3.476(5) Å, $D_{Cg3\text{-}Cg6}$ = 3.753(7) Å, $D_{Cg6\text{-}Cg6}$ = 3.577(7) Å, and $D_{Cg6\text{-}Cg10}$ = 3.465(6) Å. (**C**) π-π stacking interactions between building blocks. The selected distances (*D*) between ring centroids are as follows: $D_{Cg1\text{-}Cg3}$ = 3.621(6) Å, $D_{Cg1\text{-}Cg5}$ = 3.645(5) Å, $D_{Cg1\text{-}Cg10}$ = 3.710(6) Å, $D_{Cg4\text{-}Cg6}$ = 3.753(7) Å, and $D_{Cg4\text{-}Cg9}$ = 3.577(7) Å. (**D**) 3D porous supramolecular structure of **π-1** viewed along the *c* axis, where one building block (yellow) surrounded by four other building blocks (blue and purple) is clearly demonstrated.

Zn(II) structural units. There are as many as 33 types of π-π stacking modes observed in **π-1** (Table 1 and fig. S3). First, two phen rings of the structural unit respectively stack with two phen rings of two adjacent structural units to form the chain building block. The π-π interactions include Cg2-Cg5 [D = 3.476(5) Å], Cg2-Cg7 [D = 3.784(5) Å], Cg2-Cg8 [D = 3.721(5) Å], Cg2-Cg11 [D = 3.700(4) Å], Cg3-Cg6 [D = 3.753(7) Å], Cg3-Cg9 [D = 3.866(6) Å], Cg6-Cg6 [D = 3.577(7) Å], Cg6-Cg10 [D = 3.465(6) Å], Cg6-Cg12 [D = 3.577(7) Å],

Table 1. π-π stacking interactions in π-1. Cg1, N1 → N2 → N3 → N4 → C8→; Cg2, N6 → C18 → C17 → C16 → C15 → C19→; Cg3, N8 → C30 → C29 → C28 → C27 → C31→; Cg4, C2 → C3 → C4 → C5 → C6 → C7→; Cg5, C12 → C13 → C14 → C15 → C19 → C20→; Cg6, C24 → C25 → C26 → C27 → C31 → C32→; Cg7, N5 → C9 → C10 → C11 → C12 → C13 → C14 → C15 → C19 → C20→; Cg8, N6 → C18 → C17 → C16 → C15 → C14 → C13 → C12 → C20 → C19→; Cg9, N7 → C21 → C22 → C23 → C24 → C25 → C26 → C27 → C31 → C32→; Cg10, N8 → C30 → C29 → C28 → C27 → C26 → C25 → C24 → C32 → C31→; Cg11, N5 → C9 → C10 → C11 → C12 → C13 → C14 → C15 → C16 → C17 → C18 → N6 → C19 → C20→; Cg12, N7 → C21 → C22 → C23 → C24 → C25 → C26 → C27 → C28 → C29 → C30 → N8 → C31 → C32→.

Entry	π-π interactions	Cg-Cg (Å)*	α (°)†	β (°)‡	Cg-plane (Å)§	Slippage (Å)‖	Symmetry operation on Cg
1	Cg1-Cg3	3.621(6)	0.0(5)	22.9	3.335(3)	1.410	$x-y, -1+x, 2-z$
2	Cg1-Cg5	3.645(5)	0.0(4)	25.3	3.015(8)/3.295(3)	1.557	$1/3+y, 2/3-x+y, 5/3-z$
3	Cg1-Cg10	3.710(6)	0.0(4)	25.8	3.340(3)	1.615	$x-y, -1+x, 2-z$
4	Cg2-Cg5	3.475(5)	0.6(4)	8.8	3.434(3)	0.534	$5/3-x, 1/3-y, 4/3-z$
5	Cg2-Cg7	3.784(5)	1.1(3)	25.5	3.432(3)/3.415(3)	1.629	$5/3-x, 1/3-y, 4/3-z$
6	Cg2-Cg8	3.721(5)	0.3(3)	22.4	3.434(3)/3.440(2)	1.417	$5/3-x, 1/3-y, 4/3-z$
7	Cg2-Cg11	3.700(4)	0.7(3)	22.2	3.427(3)3.425(2)	1.399	$5/3-x, 1/3-y, 4/3-z$
8	Cg3-Cg6	3.753(7)	1.4(6)	24.4	3.388(5)/3.419(5)	1.547	$5/3-x, 1/3-y, 7/3-z$
9	Cg3-Cg9	3.866(6)	2.2(5)	29.0	3.373(5)/3.380(4)	1.877	$5/3-x, 1/3-y, 7/3-z$
10	Cg4-Cg6	3.920(6)	0.0(5)	24.9	3.557(3)	1.648	$x-y, -1+x, 2-z$
11	Cg4-Cg9	3.914(5)	0.0(3)	23.9	3.578(3)	1.587	$x-y, -1+x, 2-z$
12	Cg5-Cg2	3.476(5)	0.6(4)	8.9	3.434(3)	0.536	$5/3-x, 1/3-y, 4/3-z$
13	Cg5-Cg8	3.627(4)	0.3(3)	18.6	3.433(2)/3.438(2)	1.154	$5/3-x, 1/3-y, 4/3-z$
14	Cg6-Cg3	3.753(7)	1.4(6)	25.5	3.419(5)/3.387(5)	1.616	$5/3-x, 1/3-y, 7/3-z$
15	Cg6-Cg6	3.577(7)	0.0(6)	17.7	3.408(5)	1.087	$5/3-x, 1/3-y, 7/3-z$
16	Cg6-Cg10	3.465(6)	0.6(5)	11.5	3.398(5)/3.395(4)	0.689	$5/3-x, 1/3-y, 7/3-z$
17	Cg6-Cg12	3.674(6)	0.6(5)	22.9	3.397(5)/3.383(3)	1.431	$5/3-x, 1/3-y, 7/3-z$
18	Cg7-Cg2	3.784(5)	1.1(3)	24.9	3.416(3)/3.432(3)	1.594	$5/3-x, 1/3-y, 4/3-z$
19	Cg8-Cg2	3.721(5)	0.3(3)	22.7	3.441(2)/3.434(3)	1.433	$5/3-x, 1/3-y, 4/3-z$
20	Cg8-Cg5	3.627(4)	0.3(3)	18.8	3.438(2)/3.433(3)	1.169	$5/3-x, 1/3-y, 4/3-z$
21	Cg8-Cg8	3.476(4)	0.0(2)	9.0	3.433(2)	0.542	$5/3-x, 1/3-y, 4/3-z$
22	Cg8-Cg11	3.700(4)	0.4(2)	22.3	3.432(2)/3.423(2)	1.405	$5/3-x, 1/3-y, 4/3-z$
23	Cg9-Cg3	3.866(6)	2.2(5)	29.2	3.380(4)/3.373(5)	1.889	$5/3-x, 1/3-y, 7/3-z$
24	Cg9-Cg10	3.768(5)	1.4(4)	25.7	3.369(4)/3.394(4)	1.637	$5/3-x, 1/3-y, 7/3-z$
25	Cg10-Cg6	3.464(6)	0.6(5)	11.3	3.395(4)/3.397(5)	0.678	$5/3-x, 1/3-y, 7/3-z$
26	Cg10-Cg9	3.768(5)	1.4(4)	26.6	3.394(4)/3.369(4)	1.689	$5/3-x, 1/3-y, 7/3-z$
27	Cg10-Cg10	3.749(5)	0.0(4)	25.1	3.396(4)/3.396(4)	1.588	$5/3-x, 1/3-y, 7/3-z$
28	Cg10-Cg12	3.714(5)	0.8(3)	24.7	3.386(4)/3.376(3)	1.549	$5/3-x, 1/3-y, 7/3-z$
29	Cg11-Cg2	3.701(4)	0.7(3)	22.2	3.426(2)/3.427(3)	1.396	$5/3-x, 1/3-y, 4/3-z$
30	Cg11-Cg8	3.700(4)	0.4(2)	22.0	3.423(2)/3.432(2)	1.383	$5/3-x, 1/3-y, 4/3-z$
31	Cg12-Cg6	3.673(6)	0.6(5)	22.4	3.383(3)/3.396(5)	1.398	$5/3-x, 1/3-y, 7/3-z$
32	Cg12-Cg10	3.714(5)	0.8(3)	24.3	3.376(3)/3.386(4)	1.527	$5/3-x, 1/3-y, 7/3-z$
33	Cg12-Cg12	3.965(4)	0.0(2)	31.5	3.380(3)/3.381(3)	2.072	$5/3-x, 1/3-y, 7/3-z$

*Distance between ring centroids. †Dihedral angle between planes *I* and *J*. ‡Angle between Cg(*I*)-Cg(*J*) vector and normal to plane *I*.
§Perpendicular distance of Cg(*I*) on ring *J*. ‖Distance between Cg(*I*) and perpendicular projection of Cg(*J*) on ring *I*.

and so on (Fig. 1B; fig. S3, B, C, and E to L; and Table 1). These multiple strong π-π interactions endow the supramolecular chain building block with high stability. Then, the stable chain building block further connects with four equivalent chain building blocks through π-π interactions to weave a 3D porous supramolecular framework. The key π-π interactions herein involve those between the tetrazolyl ring and the phen ring—Cg1-Cg3 [D = 3.621(6) Å], Cg1-Cg5 [D = 3.645(5) Å], and Cg1-Cg10 [D = 3.710(6) Å] (Fig. 1C, fig. S3A, and Table 1)—and those between the aromatic ring and the phen ring, Cg4-Cg6 [D = 3.753(7) Å] and Cg4-Cg9 [D = 3.577(7) Å] (Fig. 1C, fig. S3D, and Table 1). Dependent on the synergistic effect of multiple π-π interactions, a 3D porous supramolecular framework of **π-1** is assembled. Thus, many π-π stacking interactions in **π-1** should be attributed to the fact that all the conjugated organic groups of the structural unit take part in the formation of π-π stacking interactions (Table 1 and fig. S3). Usually, the ring normal and the vector between the ring centroids forming an angle of about 20° up to Cg-Cg distances of 3.8 Å indicate a strong π-π stacking interaction (*30*). As most of the π-π interactions in **π-1** have shorter centroid distances [3.465(6) to 3.784(5) Å; Table 1] and the angle between the ring normal and the vector Cg-Cg is in the range of 18.6° to 22.9° (Table 1), the π-π interactions in **π-1** belong to strong π-π interactions. Such strong and multiple π-π stacking interactions significantly contribute to the stability of **π-1**. Note that with the exception of π-π stacking interactions, there are no other covalent/noncovalent interactions between Zn(II) structural units. Therefore, **π-1** represents a typical porous supramolecular π framework, which has not been reported yet to the best of our knowledge.

Thermal stability

The powder XRD measured at room temperature showed that all the peaks displayed in the pattern closely match those in the simulated one generated from the single-crystal diffraction data, which indicates that a single phase of **π-1** was formed (fig. S4A). TG analysis revealed that the guest solvent molecules in **π-1** can be released when heated to 75°C. The weight loss of 23.7% corresponds to three CH_3OH and six H_2O molecules per molecular unit in **π-1** (calculated: 24.1%; fig. S4B). With the loss of the lattice guest molecules, the color of **π-1** changes from light brown to dark green. Once the activated **π-1** is exposed to air, the color of the activated **π-1** quickly returns to light brown, exhibiting a reversible process (fig. S4C). Differential scanning calorimetry measurements showed that for **π-1**, a small endothermic peak at 85.11°C and a big endothermic peak at 128.27°C were observed (fig. S4D). For activated **π-1**, only a big endothermic peak at 127.73°C was detected (fig. S4E). These endothermic peaks correspond to the loss of guest solvents. No other endothermic peak was observed after the guest loss, showing that no structural transformations/distortions/rearrangements occurred after the guest loss. Variable-temperature powder XRD measurements demonstrated that the desolvated framework of **π-1** can remain stable, as the main diffraction pattern of **π-1** does not change from room temperature to at least 80°C (fig. S4F), at which the guest molecules in the pores are removed, as indicated by the TG result (fig. S4B).

The stability of the desolvated **π-1** was further confirmed by gas sorption measurements. As shown in fig. S4F, the pores of **π-1** cannot adsorb N_2/H_2 at 77 K and Ar at 87 K, while it can adsorb CO_2 at 195 K, exhibiting selective adsorption behavior. Considering that the pore size of **π-1** is 7.5 Å by 7.5 Å—much larger than the dynamic diameters of H_2 (2.86 Å), Ar (3.4 Å), and N_2 (3.64 Å)—the selective adsorption of **π-1** to CO_2 (3.3 Å) may be attributed to the special quadrupole moment of CO_2 (-1.4×10^{-39} Cm^2), which can induce the framework to interact with CO_2 molecules and thus increase the binding to CO_2 (*31*). The adsorption isotherm shows a type I curve, indicating the microporous characteristic of **π-1**. The maximum CO_2 uptake reaches 36.3 cm^3/g (standard temperature and pressure) at normal pressure, confirming the real existence of permanent porosity in **π-1** after the removal of the lattice guest molecules. To the best of our knowledge, **π-1** represents the first example of a porous supramolecular framework stabilized merely by intermolecular π-π stacking interactions. Although several supramolecular compounds that seem to be π frameworks have been reported, there are other noncovalent interactions, such as nonclassical hydrogen bonds, that contribute to their stability besides the π-π stacking interactions. In addition, their permanent porosities have not been investigated and verified (*32*–*34*).

Chemical stability

Besides thermal stability, the chemical stability of **π-1** was also studied (see the Supplementary Materials). As shown in fig. S5A, the powder XRD patterns of **π-1** after being respectively immersed in H_2O, methanol, ethanol, acetonitrile, benzene, etc. for 3 days are similar to those of the simulated one, demonstrating that the framework of **π-1** can remain stable in H_2O and common organic solvents. These exciting results encouraged us to further investigate its stability in aqueous solution at different pH values. The results show that the powder XRD patterns of **π-1** after the immersion in aqueous solution at pH values ranging from 3 to 12 for 3 days are similar to those of the simulated one (fig. S5B), suggesting that **π-1** is resistant to acid and base in the pH range of 3 to 12. The above results show that **π-1** has good chemical stability. This good chemical stability may be attributed to its unique structural feature. As shown in fig. S2B, the coordination portion in **π-1**, the core of complex that directly determines the compound stability, is enwrapped by hydrophobic organic moieties, avoiding the attack of solvents or acid/base to the coordination units. Therefore, **π-1** can remain stable in aqueous solution and common organic solvents, even in acidic/basic aqueous solutions.

Hg^{2+} removal

Considering the good stability and the thiolate group–modified pores, the performance of **π-1** for removing Hg^{2+} in aqueous solution was evaluated. Typically, the Hg^{2+} adsorption experiments of **π-1** were carried out by immersing 10 mg of desolvated **π-1** into 10-ml $HgCl_2$ aqueous solutions with different concentrations. As shown in Fig. 2A and fig. S6 (A to C), at a low initial concentration, **π-1** can capture almost all the Hg^{2+} in the solution. With the increase of the initial Hg^{2+} concentration, the adsorption capacity of **π-1** gradually increases. When the initial concentration of Hg^{2+} reaches 1200 mg/liter, the adsorption capacity of **π-1** to Hg^{2+} reaches a maximum value of 786.67 mg g^{-1}, corresponding to the capture of 0.927 Hg^{2+} per thiolate group in **π-1**. This result suggests that most of the thiolate groups in **π-1** bind to Hg^{2+} ions. The maximum Hg^{2+} uptake capacity of **π-1** is higher than that of most reported thiol/thio-functionalized porous materials (*35*–*38*) and comparable to that of benchmark porous materials COF-S-SH (*39*), Bio-MOF (*40*), PAF-1-SH (*41*), and POP-SH (*42*). The high Hg^{2+} uptake of **π-1** should be attributed to the high porosity and pore surface area of **π-1**, together with a large number of highly accessible thiolate groups that are well dispersed and exposed on the pore surface of **π-1**. The good performance of **π-1** for Hg^{2+}

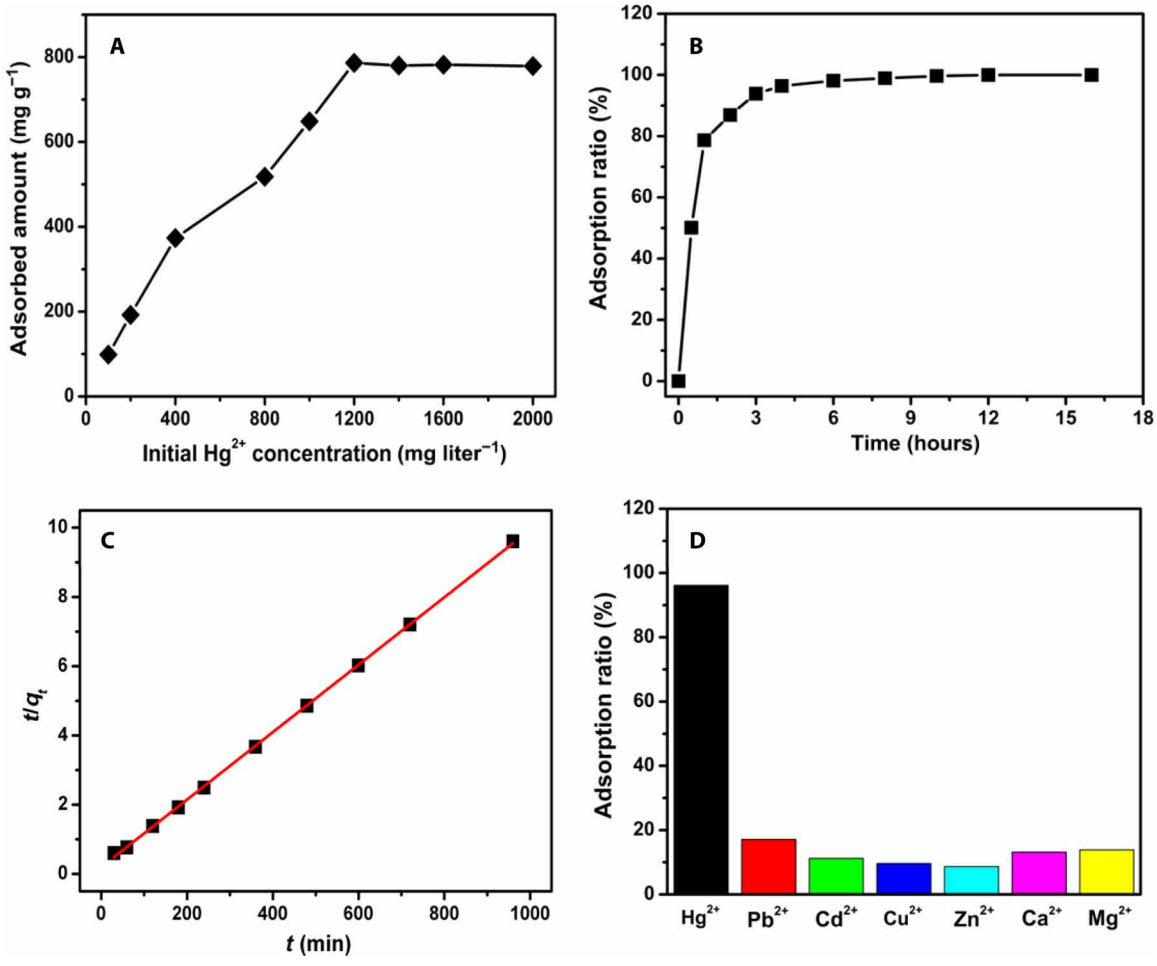

Fig. 2. Adsorption results of π-1 to Hg^{2+}. (**A**) Adsorption capacity of **π-1** to Hg^{2+} at different initial concentrations. (**B**) Adsorption process of **π-1** to Hg^{2+} at an initial concentration of 100 mg/liter. (**C**) Plot of t/q_t versus t. (**D**) Adsorption ratio of **π-1** to metal ions in a mixed solution containing Hg^{2+}, Pb^{2+}, Cd^{2+}, Cu^{2+}, Zn^{2+}, Ca^{2+}, and Mg^{2+}, with respective initial concentrations of 100 mg/liter.

removal evidently indicates that crystalline porous supramolecular materials have great potential in environmental applications.

To investigate the adsorption dynamics of **π-1** to Hg^{2+}, duplicate samples with equal amounts of desolvated **π-1** (10 mg) were soaked and stirred in a series of Hg^{2+} solutions (100 mg/liter) for 0.5, 1, 2, 3, 4, 6, 8, 10, 12, and 16 hours, respectively. After filtration, the residual Hg^{2+} contents in the filtrate were analyzed by inductively coupled plasma mass spectrometry (ICP-MS). As shown in Fig. 2B and fig. S6 (D to F), **π-1** rapidly captures Hg^{2+} at the very beginning. After 3 hours, more than 90% of Hg^{2+} in the solution was captured, and after 12 hours, 99.98% of Hg^{2+} was removed from the solution. This means that the concentration of the residual Hg^{2+} in the solution is 0.02% (0.02 mg/liter). Note that only 10 mg of **π-1** was used for the capture of 25 ml of Hg^{2+} solution (100 mg/liter). When the amount of **π-1** used was increased to 25 mg, the concentration of residual Hg^{2+} can be reduced to 1.6 μg/liter, reaching the U.S. standard of drinking water (2 μg/liter). These results demonstrate that the Hg^{2+} removal performance of **π-1** is comparable to most benchmark sorbents (*39*–*42*).

The pseudo–second-order model shown in Eq. 1 was used to fit the experimental data to further study the Hg^{2+} adsorption kinetics, where k_1 (g·mg^{-1}·min^{-1}) is the rate constant of pseudo–second-order adsorption, and q_t and q_e (mg·g^{-1}) are the amount of Hg^{2+} adsorbed at time t (min) and at equilibrium, respectively (*43*). The results shown in Fig. 2C reveal the correlation coefficient of 0.9999 and the rate constant k_1 of 1.091 mg·g^{-1} min^{-1}. Such a high correlation is sufficient to prove that the adsorption of **π-1** to Hg^{2+} belongs to the pseudo–second-order model (*44*). The k_1 value is also higher than those of most reported adsorbents for Hg^{2+} adsorption under similar conditions (*45*), suggesting an extraordinarily fast adsorption kinetics of **π-1** to Hg^{2+}.

$$\frac{t}{q_t} = \frac{1}{k_1 q_e^2} + \frac{t}{q_e} \quad (1)$$

$$K_d = \frac{(C_i - C_f)}{C_f} \times \frac{V}{m} \quad (2)$$

The distribution coefficient (K_d) is another important indicator to evaluate the adsorption performance of adsorbents. K_d is defined and calculated using Eq. 2 (*46*), where C_i and C_f represent the initial and the final equilibrium Hg^{2+} concentration, respectively, V is the volume of the treated solution (in milliliters), and m is the quantity of

the adsorbent used (in grams). Generally, a K_d value reaching 1.0×10^5 ml·g^{-1} indicates an excellent sorbent (*37*, *47*). The K_d of **π-1** for Hg^{2+} adsorption was calculated to be 4.99×10^6 ml g^{-1}. This value is more than 50 times larger than the standard value and only smaller than that of PAF-1-SH (*41*). This result reflects the superabsorbent property of **π-1** for Hg^{2+} solutions.

Besides Hg^{2+}, **π-1** also exhibits adsorption ability for other metal ions such as Pb^{2+}, Cd^{2+}, Cu^{2+}, Zn^{2+}, Ca^{2+}, and Mg^{2+} under the same conditions, with adsorption ratios of 83.32, 46.49, 62.48, 26.89, 38.42, and 49.64%, respectively (fig. S7, A to C). To investigate the adsorption selectivity of **π-1**, we prepared and used a mixture containing $HgCl_2$, $PbCl_2$, $CdCl_2$, $CuCl_2$, $ZnCl_2$, $CaCl_2$, and $MgCl_2$ instead of a single–metal ion solution. As shown in Fig. 2D and fig. S7 (G to I), **π-1** still shows strong capture performance to Hg^{2+}, with an adsorption ratio as high as 96.78%. In contrast, **π-1** exhibits low adsorption capacity to Pb^{2+}, Cd^{2+}, Cu^{2+}, Zn^{2+}, Ca^{2+}, and Mg^{2+}, with adsorption ratios of 17.15, 11.25, 9.63, 8.68, 13.15, and 13.84%, respectively. These observations demonstrated that other ions do not interfere with the adsorption capacity of **π-1** for Hg^{2+}. To the best of our knowledge, **π-1** is the first supramolecular sorbent that shows such high adsorption selectivity to Hg^{2+}.

To investigate the possible influence of metal salt solubilities on the adsorption property of **π-1**, we carried out the ion adsorption experiments by using nitrate salts [$Hg(NO_3)_2$, $Pb(NO_3)_2$, $Cd(NO_3)_2$, $Cu(NO_3)_2$, $Zn(NO_3)_2$, $Ca(NO_3)_2$, and $Mg(NO_3)_2$] instead of the corresponding chloride salts. As shown in fig. S7 (D to F), the adsorption amounts of **π-1** to single metal ion by using nitrate salts is similar to that using chloride salts (fig. S7, A to C). The adsorption selectivity of **π-1** to the mixed metal ion by using nitrate salts is also similar to that by using chloride salts (fig. S7, G to I). These results indicate that the solubility differences of these tested metal salts have limited influence on the adsorption properties of **π-1**, which may be ascribed to the very low concentration of each metal salt. At a concentration of 100 mg/liter, all the metal salts tested can completely dissolve and dissociate.

The recyclability of **π-1** for removing Hg^{2+} from aqueous solution was further examined. As shown in fig. S8A, the framework of **π-1** remained stable after adsorbing Hg^{2+}, which was also evidenced by the scanning electron microscopy (SEM) results, where the same morphology as the one without Hg^{2+} uptake was observed (fig. S8, C and D). After four runs of the adsorption-desorption cycle, the adsorption performance of **π-1** on Hg^{2+} removal barely decreases (fig. S8E), and the framework of **π-1** also remained intact (fig. S8B). The CO_2 sorption isotherms of **π-1** after the Hg^{2+} adsorption test are also similar to those before the Hg^{2+} adsorption test (fig. S8F), which further confirms the framework stability of **π-1**. These results illustrate that **π-1** has good stability and recyclability. The good reusability of **π-1** in Hg^{2+} removal can be attributed to its unique structural feature; that is, the coordination portions of the structure are enwrapped by hydrophobic organic moieties (Fig. 2B). As the capture of Hg^{2+} occurs on the pore surface of **π-1** and because there are no direct contacts and interactions with the coordination portions that directly determine the stability of the whole framework, **π-1** can retain its framework stability during the Hg^{2+} adsorption-desorption process and its recyclability during Hg^{2+} removal without any decrease in adsorption performance and efficiency. The good recycle performance of **π-1** during Hg^{2+} removal is comparable to most porous absorbent materials with a state-of-the-art Hg^{2+} adsorption function (*41*, *42*, *48*). The high Hg^{2+} uptake, selective adsorption ability against interference, and good recycle performance would enable **π-1** to become a potential sorbent in water purification.

DISCUSSION

In summary, we have assembled a porous crystalline framework stabilized merely by π-π stacking interactions. Without other covalent/noncovalent interactions, this stable π framework could serve as concrete evidence that π-π stacking interactions are non-negligible forces for stabilizing porous supramolecular frameworks, especially in HOFs. Notably, the thiolate-functionalized **π-1** shows exceptional chemical stability not only in water and common organic solvents but also in acidic and basic aqueous solutions. As a result, **π-1** exhibits excellent Hg^{2+} removal performance in terms of uptake capacity, selectivity, and recyclability comparable to reported pioneering Hg^{2+} sorbents.

MATERIALS AND METHODS

Materials and measurements

All the chemicals were commercially available and used without further purification. Fourier transform IR (FTIR) spectra were recorded on a PerkinElmer Frontier Mid-IR-FTIR apparatus in ATR or transmittance mode. Powder XRD measurements were performed on a Bruker D8 Focus diffractometer using the CuKα radiation. TG analyses were carried out on a BOIF WCT-2C Thermogravimetry Analyzer at N_2 atmosphere. Gas sorption measurements were performed on a BELSORP-max automatic volumetric adsorption apparatus. ICP-MS tests were performed on a HORIBA Ultima Expert ICP Optical Emission Spectrometer and an Agilent 7900 ICP-MS instrument. Atomic fluorescence spectroscopy (AFS) measurements were carried out on a Jitian AFS-922 double-channel atomic fluorescence spectrometer. Examination of the acetate (Ac^-) was performed using Metrohm Eco IC ion chromatography.

Preparation of π-1

A mixture of 0.2 mmol of $Zn(Ac)_2{\cdot}2H_2O$ (0.0439 g), 0.1 mmol of 1,10-phenanthroline monohydrate (phen; 0.018 g), 0.1 mmol of 1-(4-carboxyphenyl)-5-mercapto-1*H*-tetrazole (H_2L; 0.022 g), and 12 ml of CH_3OH/H_2O mixture (v:v = 1:1) was stirred at room temperature for 10 min. After adjusting the pH to 7.6 by adding triethylamine, the mixture was transferred to a Teflon-lined stainless steel autoclave and heated at 105°C for 72 hours. The autoclave was cooled to room temperature at a rate of 10°C·hour^{-1}. The mixture was filtered, and the resulting colorless clear filtrate was allowed to stand at room temperature for 2 to 3 days; rod crystals of **π-1** were obtained. The crystals were collected by filtration and dried in air. Yield: 73% based on H_2L. Elemental analyses calcd (%) for $C_{35}H_{44}N_8O_{11}SZn$ (**π-1**): C, 49.44; H, 5.22; N, 13.18. Found: C, 49.12; H, 5.05; N, 13.27. IR (KBr, cm^{-1}): 3421(s), 3057(w), 2364(m), 2341(m), 1612(vs), 1558(s), 1516(vs), 1432(vs), 1377(vs), 1342(s), 1274(m), 1222(w), 1142(w), 1102(s), 1011(w), 848(vs), 785(m), 725(vs), 642(w), 472(w).

Hg^{2+} removal measurements

Ten milligrams of pretreated **π-1** was added to a 25-ml glass vial containing 10 ml of $HgCl_2$ solution with a concentration of 100 mg/liter. After stirring for a certain period, the solution was filtered. The resulting filtrate was tested by ICP-MS/AFS to check the residual amount of Hg^{2+}. The resulting crystals were tested by SEM and

powder XRD. The procedures for other ion removal measurements were similar to that for Hg^{2+} removal by using $PbCl_2$, $CdCl_2$, $CuCl_2$, $ZnCl_2$, $CaCl_2$, or $MgCl_2$ solution (100 mg/liter) instead of Hg^{2+} solution (100 mg/liter). After stirring for 12 hours, the solution was filtered and the residual ion concentration in the filtrate was tested by ICP-MS. The procedure for metal ion removal experiments of **π-1** using nitrate salts is similar to that using chloride salts.

Maximum Hg^{2+} uptake measurements

Ten milligrams aliquots of pretreated **π-1** were added to 25-ml glass vials containing 10 ml of $HgCl_2$ solution with concentrations of 100, 200, 400, 800, 1000, 1200, 1600, and 2000 mg/liter. After stirring for 12 hours, the solution was filtered. The resulting filtrate was tested by ICP-MS to check the residual amount of Hg^{2+}.

Selective adsorption tests

The procedure was similar to that described above by using a 10-ml mixture containing $HgCl_2$, $PbCl_2$, $CdCl_2$, $CuCl_2$, $ZnCl_2$, $CaCl_2$, and $MgCl_2$ with concentrations of 100 mg/liter instead of 10 ml of $HgCl_2$ solution (100 mg/liter). After stirring for 12 hours, the mixture was filtered, and the filtrate was measured by ICP-MS to check the concentration of each ion in the filtrate. In addition, a 10-ml mixture containing $Hg(NO_3)_2$, $Pb(NO_3)_2$, $Cd(NO_3)_2$, $Cu(NO_3)_2$, $Zn(NO_3)_2$, $Ca(NO_3)_2$, and $Mg(NO_3)_2$ with concentrations of 100 mg/liter instead of the corresponding chloride salts was prepared and used to further confirm the influence of the solubilities of metal salts to the selective adsorption properties of **π-1**.

Recycle tests

After the Hg^{2+} adsorption experiment, the crystalline solid was isolated by centrifugation. The obtained solid was soaked in a HCl solution (pH 5.6) for 6 hours, then isolated by centrifugation and dried in a vacuum oven at 50°C, and used for the next run of the Hg^{2+} adsorption experiment.

SUPPLEMENTARY MATERIALS

Supplementary material for this article is available at http://advances.sciencemag.org/cgi/content/full/6/2/eaax9976/DC1

Supplementary Methods

Table S1. Crystal data and structure refinements for π-1.

Table S2. Selected bond length (Å) and angle (°) for π-1.

Fig. S1. Morphology and composition characterization of π-1.

Fig. S2. 3D porous supramolecular structures of π-1 viewed along the *c* axis.

Fig. S3. π-π stacking interactions and corresponding distances (*D*) between ring centroids in π-1.

Fig. S4. Thermal stability of π-1.

Fig. S5. Chemical stability of π-1.

Fig. S6. Repeated experiments of π-1 for adsorbing Hg^{2+}.

Fig. S7. Repeated experiments of π-1 for selectively capturing Hg^{2+}.

Fig. S8. The durability of π-1 during Hg^{2+} adsorption.

REFERENCES AND NOTES

1. C. J. Pedersen, The discovery of crown ethers (Nobel lecture). *Angew. Chem. Int. Ed.* **27**, 1021–1027 (1988).
2. J.-M. Lehn, Supramolecular chemistry—Scope and perspectives molecules, supermolecules, and molecular devices (Nobel lecture). *Angew. Chem. Int. Ed.* **27**, 89–112 (1988).
3. D. J. Cram, The design of molecular hosts, guests, and their complexes (Nobel lecture). *Angew. Chem. Int. Ed.* **27**, 1009–1020 (1988).
4. J. M. Lehn, *Supramolecular Chemistry* (VCH, 1995).
5. R. S. Mulliken, Electronic population analysis on LCAO–MO molecular wave functions. II. Overlap populations, bond orders, and covalent bond energies. *J. Chem. Phys.* **23**, 1841–1846 (1955).
6. K. Wendler, J. Thar, S. Zahn, B. Kirchner, Estimating the hydrogen bond energy. *J. Phys. Chem. A* **114**, 9529–9536 (2010).
7. Y. Zhao, D. G. Truhlar, Noncovalent interaction energies of biological importance. *J. Chem. Theory Comput.* **3**, 289–300 (2007).
8. E. R. Johnson, S. Keinan, P. Mori-Sánchez, J. Contreras-García, A. J. Cohen, W. Yang, Revealing noncovalent interactions. *J. Am. Chem. Soc.* **132**, 6498–6506 (2010).
9. R.-B. Lin, Y. He, P. Li, H. Wang, W. Zhou, B. L. Chen, Multifunctional porous hydrogen-bonded organic framework materials. *Chem. Soc. Rev.* **48**, 1362–1389 (2019).
10. I. Hisaki, Y. Suzuki, E. Gomez, Q. Ji, N. Tohnai, T. Nakamura, A. Douhal, Acid responsive hydrogen-bonded organic frameworks. *J. Am. Chem. Soc.* **141**, 2111–2121 (2019).
11. Z. Bao, D. Xie, G. Chang, H. Wu, L. Li, W. Zhou, H. Wang, Z. Zhang, H. Xing, Q. Yang, M. J. Zaworotko, Q. Ren, B. Chen, Fine tuning and specific binding sites with a porous hydrogen-bonded metal-complex framework for gas selective separations. *J. Am. Chem. Soc.* **140**, 4596–4603 (2018).
12. I. Hisaki, Y. Suzuki, E. Gomez, B. Cohen, N. Tohnai, A. Douhal, Docking strategy to construct thermostable, single-crystalline, hydrogen-bonded organic framework with high surface area. *Angew. Chem. Int. Ed.* **57**, 12650–12655 (2018).
13. Q. Yin, P. Zhao, R.-J. Sa, G.-C. Chen, J. Lü, T.-F. Liu, R. Cao, An ultra-robust and crystalline redeemable hydrogen-bonded organic framework for synergistic chemo-photodynamic therapy. *Angew. Chem. Int. Ed.* **57**, 7691–7696 (2018).
14. J. Luo, J.-W. Wang, J.-H. Zhang, S. Lai, D.-C. Zhong, Hydrogen-bonded organic frameworks: Design, structures and potential applications. *CrystEngComm* **20**, 5884–5898 (2018).
15. F. Hu, C. Liu, M. Wu, J. Pang, F. Jiang, D. Yuan, M. Hong, An ultrastable and easily regenerated hydrogen-bonded organic molecular framework with permanent porosity. *Angew. Chem. Int. Ed.* **56**, 2101–2104 (2017).
16. A. Karmakar, R. Illathvalappil, B. Anothumakkool, A. Sen, P. Samanta, A. V. Desai, S. Kurungot, S. K. Ghosh, Hydrogen-bonded organic frameworks (HOFs): A new class of porous crystalline proton-conducting materials. *Angew. Chem. Int. Ed.* **55**, 10667–10671 (2016).
17. Y. He, S. Xiang, B. Chen, A microporous hydrogen-bonded organic framework for highly selective C_2H_2/C_2H_4 separation at ambient temperature. *J. Am. Chem. Soc.* **133**, 14570–14573 (2011).
18. X.-Z. Luo, X.-J. Jia, J.-H. Deng, J.-L. Zhong, H.-J. Liu, K.-J. Wang, D.-C. Zhong, A microporous hydrogen-bonded organic framework: Exceptional stability and highly selective adsorption of gas and liquid. *J. Am. Chem. Soc.* **135**, 11684–11687 (2013).
19. M. Mastalerz, I. M. Oppel, Rational construction of an extrinsic porous molecular crystal with an extraordinary high specific surface area. *Angew. Chem. Int. Ed.* **51**, 5252–5255 (2012).
20. A. I. Cooper, Molecular organic crystals: From barely porous to really porous. *Angew. Chem. Int. Ed.* **51**, 7892–7894 (2012).
21. Z. Wang, J. Yu, R. Xu, Needs and trends in rational synthesis of zeolitic materials. *Chem. Soc. Rev.* **41**, 1729–1741 (2012).
22. G. Maurin, C. Serre, A. Cooper, G. Férey, The new age of MOFs and of their porous-related solids. *Chem. Soc. Rev.* **46**, 3104–3107 (2017).
23. A. P. Côté, A. I. Benin, N. W. Ockwig, M. O'Keeffe, A. J. Matzger, O. M. Yaghi, Porous, crystalline, covalent organic frameworks. *Science* **310**, 1166–1170 (2005).
24. C. G. Bezzu, M. Helliwell, J. E. Warren, D. R. Allan, N. B. McKeown, Heme-like coordination chemistry within nanoporous molecular crystals. *Science* **327**, 1627–1630 (2010).
25. I. A. Gass, B. Moubaraki, S. K. Langley, S. R. Batten, K. S. Murray, A π–π 3D network of tetranuclear μ_2/μ_3-carbonato Dy(III) bis-pyrazolylpyridine clusters showing single molecule magnetism features. *Chem. Commun.* **48**, 2089–2091 (2012).
26. J. H. Chong, S. J. Ardakani, K. J. Smith, M. J. MacLachlan, Triptycene-based metal salphens—Exploiting intrinsic molecular porosity for gas storage. *Chem. A Eur. J.* **15**, 11824–11828 (2009).
27. H. Fukunaga, H. Miyasaka, Magnet design by integration of layer and chain magnetic systems in a π-stacked pillared layer framework. *Angew. Chem. Int. Ed.* **54**, 569–573 (2015).
28. J. Guo, Y. Xu, S. Jin, L. Chen, T. Kaji, Y. Honsho, M. A. Addicoat, J. Kim, A. Saeki, H. Ihee, S. Seki, S. Irle, M. Hiramoto, J. Gao, D. Jiang, Conjugated organic framework with three-dimensionally ordered stable structure and delocalized π clouds. *Nat. Commun.* **4**, 2736 (2013).
29. L. J. Bellamy, *The Infrared Spectra of Complex Molecules* (Wiley, 1958).
30. C. Janiak, A critical account on π–π stacking in metal complexes with aromatic nitrogen-containing ligands. *J. Chem. Soc. Dalton Trans.* 3885–3896 (2000).
31. J.-R. Li, J. Sculley, H.-C. Zhou, Metal-organic frameworks for separations. *Chem. Rev.* **112**, 869–932 (2012).
32. S. Cai, H. Shi, Z. Zhang, X. Wang, H. Ma, N. Gan, Q. Wu, Z. Cheng, K. Ling, M. Gu, C. Ma, L. Gu, Z. An, W. Huang, Hydrogen-bonded organic aromatic frameworks for ultralong phosphorescence by intralayer π–π interactions. *Angew. Chem. Int. Ed.* **57**, 4005–4009 (2018).
33. T. N. Hooper, R. Inglis, M. A. Palacios, G. S. Nichol, M. B. Pitak, S. J. Coles, G. Lorusso, M. Evangelisti, E. K. Brechin, CO_2 as a reaction ingredient for the construction of metal cages: A carbonate-panelled $[Gd_6Cu_3]$. tridiminished icosahedron. *Chem. Commun.* **50**, 3498–3500 (2014).

34. D. Anselmo, G. Salassa, E. C. Escudero-Adán, E. Martin, A. W. Kleij, Merging catalysis and supramolecular aggregation features of triptycene based Zn(salphen)s. *Dalton Trans.* **42**, 7962–7970 (2013).
35. X. Feng, G. E. Fryxell, L.-Q. Wang, A. Y. Kim, J. Liu, K. M. Kemner, Functionalized monolayers on ordered mesoporous supports. *Science* **276**, 923–926 (1997).
36. J. Liu, X. Feng, G. E. Fryxell, L.-Q. Wang, A. Y. Kim, M. Gong, Hybrid mesoporous materials with functionalized monolayers. *Adv. Mater.* **10**, 161–165 (1998).
37. Y. Shin, G. E. Fryxell, W. Um, K. Parker, S. V. Mattigod, R. Skaggs, Sulfur-functionalized mesoporous carbon. *Adv. Funct. Mater.* **17**, 2897–2901 (2007).
38. K.-K. Yee, N. Reimer, J. Liu, S.-Y. Cheng, S.-M. Yiu, J. Weber, N. Stock, Z. Xu, Effective mercury sorption by thiol-laced metal–organic frameworks: In strong acid and the vapor phase. *J. Am. Chem. Soc.* **135**, 7795–7798 (2013).
39. Q. Sun, B. Aguila, J. Perman, L. D. Earl, C. W. Abney, Y. Cheng, H. Wei, N. Nguyen, L. Wojtas, S. Ma, Postsynthetically modified covalent organic frameworks for efficient and effective mercury removal. *J. Am. Chem. Soc.* **139**, 2786–2793 (2017).
40. M. Mon, F. Lloret, J. Ferrando-Soria, C. Martí-Gastaldo, D. Armentano, E. Pardo, Selective and efficient removal of mercury from aqueous media with the highly flexible arms of a BioMOF. *Angew. Chem. Int. Ed.* **55**, 11167–11172 (2016).
41. B. Li, Y. Zhang, D. Ma, Z. Shi, S. Ma, Mercury nano-trap for effective and efficient removal of mercury(II) from aqueous solution. *Nat. Commun.* **5**, 5537 (2014).
42. B. Aguila, Q. Sun, J. A. Perman, L. D. Earl, C. W. Abney, R. Elzein, R. Schlaf, S. Ma, Efficient mercury capture using functionalized porous organic polymer. *Adv. Mater.* **29**, 1700665 (2017).
43. Y.-S. Ho, Review of second-order models for adsorption systems. *J. Hazard. Mater.* **136**, 681–689 (2006).
44. F.-C. Wu, R. L. Tseng, R.-S. Juang, Kinetic modeling of liquid-phase adsorption of reactive dyes and metal ions on chitosan. *Water Res.* **35**, 613–618 (2001).
45. P. A. Kobielska, A. J. Howarth, O. K. Farha, S. Nayak, Metal–organic frameworks for heavy metal removal from water. *Coord. Chem. Rev.* **358**, 92–107 (2018).
46. D. D. Do, *Adsorption Analysis: Equilibria and Kinetics* (Imperial College Press, 1998).
47. M. J. Manos, V. G. Petkov, M. G. Kanatzidis, $H_{2x}Mn_xSn_{3-x}S_6$ (x = 0.11–0.25): A novel reusable sorbent for highly specific mercury capture under extreme pH conditions. *Adv. Funct. Mater.* **19**, 1087–1092 (2009).
48. C. W. Abney, J. C. Gilhula, K. Lu, W. Lin, Metal-organic framework templated inorganic sorbents for rapid and efficient extraction of heavy metals. *Adv. Mater.* **26**, 7993–7997 (2014).

Acknowledgments

Funding: This work was financially supported by the National Key R&D Program of China (2017YFA0700104), the National Natural Science Foundation of China (21931007 and 21861001), and 111 Project of China (D17003). **Author contributions:** D.-C.Z. conceived and designed the study. J.L., Y.-L.M., and S.L. performed the experiments. J.-H.D. and D.-C.Z. guided the experiments and analyzed the results. Y.-N.G. determined the crystal structure. J.-H.D., J.L., D.-C.Z., and T.-B.L. wrote and revised the paper. All the authors contributed to the overall scientific interpretation and edited the manuscript. **Competing interests:** The authors declare that they have no competing interests. **Data and materials:** All data needed to evaluate the conclusions in the paper are present in the paper and/or the Supplementary Materials. Additional data related to this paper may be requested from the authors. The x-ray crystallographic coordinates for π-1 have been deposited at the Cambridge Crystallographic Data Centre (CCDC), with a deposition number of CCDC 1868705. These data can be obtained free of charge from CCDC via www.ccdc.cam.ac.uk/data_request/cif.

Submitted 10 May 2019
Accepted 11 November 2019
Published 10 January 2020
10.1126/sciadv.aax9976

Citation: J.-H. Deng, J. Luo, Y.-L. Mao, S. Lai, Y.-N. Gong, D.-C. Zhong, T.-B. Lu, π-π stacking interactions: Non-negligible forces for stabilizing porous supramolecular frameworks. *Sci. Adv.* **6**, eaax9976 (2020).

π-π stacking interactions: Non-negligible forces for stabilizing porous supramolecular frameworks

Ji-Hua Deng, Jie Luo, Yue-Lei Mao, Shan Lai, Yun-Nan Gong, Di-Chang Zhong and Tong-Bu Lu

Sci Adv **6** (2), eaax9976.
DOI: 10.1126/sciadv.aax9976